Characterization of Voids Formed During Liquid Impregnation of Nonwoven Multifilament Glass Networks as Related to Composite Processing

Anant D. Mahale, Robert K. Prud'homme and Ludwig Rebenfeld

TRI/Princeton, and Dept. of Chemical Engineering

Princeton University

Princeton, New Jersey 08544 USA

ABSTRACT

A technique based on matching the refractive index of an invading liquid to that of a fiber mat has been used to study entrapment of air ('voids') that occurs during forced in-plane radial flow into nonwoven multifilament glass networks. The usefulness of this technique is demonstrated in quantifying and mapping the air pockets. Experiments with a series of fluids with surface tensions varying from $28x10^{-3}$ to $36x10^{-3}$ N/m, viscosities from $45x10^{-3}$ to $290x10^{-3}$ Pa.s, and inlet flow rates from $0.15x10^{-6}$ to $0.75x10^{-6}$ m^3/s, have shown that void content is a function of the capillary number characterizing the flow process. A critical value of capillary number, $Ca = 2.5x10^{-3}$, identifies a zone below which void content increases exponentially with decreasing capillary number. Above this critical value, negligible entrapment of voids is observed. Similar experiments carried out on surface treated nonwoven mats spanning a range of equilibrium contact angles from 20^o to 78^o, have shown that there is a critical contact angle above which negligible entrapment is observed. Below this value, there is no apparent effect of contact angle on the void fraction - capillary number relationship described earlier. Studies on the effect of filament wettability, and fluid velocity and viscosity on the size of the entrapment (voids) have also been carried out. These indicate that larger sized entrapments which envelop more than one pore are favored by a low capillary number in comparison to smaller, pore level bubbles. Experiments were carried out on deformed mats - imposing high permeability spots at regular intervals on a background of low permeability. The effect of these spatial fluctuations in heterogeneity of the mat on entrapment is currently being studied.

INTRODUCTION

The resin transfer molding (RTM) process for fabricating fiber reinforced composites requires that a high viscosity liquid resin be forced to penetrate a dense fibrous network (woven or nonwoven). Incomplete penetration of the network by resin leads to permanent entrapment of air in the cured product which has a detrimental effect on its mechanical properties[1,2]. Air pockets entrapped during flow are referred to as 'voids' in keeping with the nomenclature followed by previous researchers. Volatiles arising from the resin system may also cause void formation, but we do not address voids of this nature. Voids of any kind are undesirable, since they act as stress-concentration sites and promote premature failure of the composite. The effects of voids on structural properties have been reported by previous researchers[2,3,4,5].

Voids have been classified as interstitial voids, planar voids (voids between layers of filaments), and general large voids (voids crossing many filament layers)[4]. An investigation on the origin of voids, especially interstitial voids, has been reported by Bascom and Romans[6]. Researchers have used techniques such as density measurements, water absorption, micrography, ultrasonic scan, and radiography to determine void

content. An appraisal and detailed description of these methods has been documented by Judd and Wright[2]. We have previously reported an optical technique for visualization and quantification of air pockets formed during liquid impregnation of a fiber network[7]. This technique involves using a liquid with refractive index identical to that of the filaments composing the network. Fibers in regions saturated with liquid are "optically" dissolved, revealing unoccupied space (voids) that can be distinguished by dark boundaries. A similar technique has been used for investigation of leaks in fiber glass reinforcement of pressure vessels [8]. In this paper we describe experimental work carried out on multifilament glass fiber networks using this technique to study the effect of process variables, fluid properties, and network characteristics on the quantity and nature of air entrapment.

NOMENCLATURE

h = spacing between plates of flow-cell [mat thickness]

m = mass per unit area of mat (Kg/m^2)

m_t = total mass of mat (Kg)

v = interstitial velocity of liquid (m/s)

Δx = fluctuation in value of x (units of x)

V_g = Volume occupied by glass filaments (m^3)

V_t = Total volume occupied by glass mat (m^3)

V_h = Total volume occupied by holes or artificially created pores in the glass mat (m^3)

Greek

ε = bulk porosity (-)

ε_h = porosity due to large holes or artificially created pores(-)

ε_p = porosity due to ordinary pores(-)

γ = surface tension of liquid (N/m)

μ = viscosity of fluid (Kg/m.s)

θ = equilibrium advancing contact angle (radians)

ρ_g = density of glass filaments (Kg/m^3)

EXPERIMENTAL METHODS

In-plane Radial Flow Experiment

A radial in-plane flow geometry is chosen for studying air entrapment under constant inlet flow rates. The main advantages of this geometry are that it closely emulates a 2- dimensional flow system, and that it provides a range of liquid velocities within the same experiment. For the flow rates used, the sample is sufficiently thin to eliminate gravity effects on liquid flow. The experimental system is shown in Figure 1. The system includes a syringe pump which is used to force the liquid through a center-hole into a nonwoven network compressed to a known thickness between parallel glass plates. The refractive index of the invading liquid is adjusted to be equal to that of the glass filaments in the network in order to reveal unoccupied space (voids) that are distinguished by dark boundaries[7]. Motion of the invading liquid, made visible by a light source below the flow apparatus, is captured through a microscope by a camera placed vertically on top, and recorded in real time. The apparatus is placed on a horizontal open linear motion X-Y stage, programmed to scan the network after complete impregnation with liquid. The experimental procedure is described in detail below:

(i) A centerhole, 0.3 cm diameter, is punched into a 15 cm x 15 cm nonwoven glass filament network (supplied by PPG Industries, P.O.Box 2844, Pittsburgh, PA 15230) which is compressed between two clear glass plates with clamps. Spacers of known thickness are placed on two opposing sides of the mat.

(ii) The stainless steel syringe (3.18 cm diameter, 25.4 cm stroke, Dev-Air Corp., P.O.Box 30, Paoli, PA 19301) is filled with the refractive-index matching liquid, with care to avoid entrapment of air bubbles in the syringe and connecting flow lines.

(iii) Setting on the syringe pump (Harvard Apparatus Co. Dover, Mass., Ser No: 6091) is adjusted to the required flow rate.

(iv) A CCTV camera (Sanyo, VDC 3800 Video Corp. of America, P.O.Box 5480, 7 Veronica Ave., Somerset, NJ 08873) is used with a television zoom lens (Tokina, 12.5-75 mm, F1.8, 6X). Intensity of the light source is adjusted to obtain a sharp picture of the mat on a 13 inch television monitor. Experiments are carried out in a darkened room to avoid reflection of external light from the glass surface.

(v) Outlet of the syringe pump is connected to a pneumatically operated three way valve which toggles between the flow-cell inlet and purge. A light emitting diode (LED) is used to indicate when the the flow-cell inlet is connected to the pump. This is placed in the field of view of the CCTV camera which records the experiment on a VCR (Panasonic Omnivision VHS-9600).

(vi) Before beginning the experiment, all lines are completely filled with the operating fluid up to the centerhole of the fiber mat. The three-way valve is positioned so as to isolate the flow-cell (LED off) and the video recorder and pump are started. The valve is then switched, turning the LED on to indicate flow of liquid into the network. Flow is continued until the entire mat is saturated with liquid. The video recorded experiment enables one to analyze temporal data in the form of radial position of the fluid front as a function of penetration time which gives the interstitial velocity as a function of radial position.

The analysis of recorded experiments utilizes an image analysis system developed at TRI/Princeton, which combines image acquisition hardware with prepackaged libraries of graphics routines and data manipulation programs.

Void Analysis

The quantity of entrapped air at any location is expressed in the form of a void fraction, which is defined as a ratio of the volume of air entrapped to the total volume. Volumes are calculated by multiplying the measured area of the air pocket by the thickness of the mat. The air pockets are assumed to extend across the thickness of the mat in this calculation. In case of small bubbles, this assumption gives an overestimate of the actual void fraction.

Other information about voids includes their size distribution. For this purpose, three size ranges are chosen as follows:

$x_1 = [N_1/N_t]$ - Ratio of the number of entrapments in the range of sizes less than 0.32×10^{-9} m^3 per unit area of mat to the total number of bubbles per unit area. This is a range of sizes extending up to about ten times the mean pore size in the mat [0.02×10^{-9} m^3].

$x_2 = [N_2/N_t]$ - Ratio of the number of entrapments in the range of sizes from 0.32×10^{-9} m^3 to 1.9×10^{-9} m^3 per unit area of mat to the total number of bubbles per unit area.

$x_3 = [N_3/N_t]$ - Ratio of the number of entrapments in the range of sizes greater than 1.9×10^{-9} m^3 per unit area of mat to the total number of bubbles per unit area.

The experimental procedure for void analysis is as follows:

(i) The CCTV camera with an 8X magnification lens is mounted on the eyepiece of a microscope (Olympus) with a magnification range of 0.7 to 4.0 and is used for photographing the network at a total magnification of 645X. At this magnification, the smallest measurable air pocket is of size $0.1 \times 10^{-6} m^2$ within an error of 5%. Assuming air pockets to be cylindrical, with height equal to that of the spacing between the plates of the flow cell, the measured area of air entrapment corresponds to a void volume of $0.05 \times 10^{-9} m^3$. Smaller air pockets can be identified but cannot be quantified without greater experimental error.

(ii) The horizontal open frame linear motion stage (Daedal Inc., P.O.Box G, Harrison City, PA 15636) is programmed to scan and photograph the saturated network to provide a record of each frame for subsequent analysis. The total domain of study is a 0.112 m x 0.121 m rectangle.

(iii) The recording of the experiment is played back and a frame is captured on the RGB monitor for study. Each micrograph of the high magnification scan obtained in the experiment is analyzed to obtain the area covered by voids. This is done by enclosing each void by a boundary, filling it with black pixels, and counting the enclosed pixels. This procedure is repeated for all voids in each frame.

(iv) The radial position of each micrograph is taken as the distance of its center from the center hole. Void areas measured at equal radial positions are arithmetically averaged to obtain the mean void area at that radial position. This gives the void fraction as a function of radial position and liquid velocity.

(v) In the analysis of each micrograph, a classification table is maintained to record the size distribution of air entrapments. Data from micrographs at the same radial position are averaged to obtain a relationship between void sizes and fluid velocity.

Characterization of Fluids

Refractive index, viscosity and surface tension characterize the fluids used in the experiments. Wettability of filaments composing the network can be quantified in terms of an equilibrium contact angle formed by the liquid meniscus with the solid surface.

Aqueous zinc iodide solutions were found to give refractive indices in the range of that of glass, depending upon concentration. These solutions were observed to be effective in detecting air pockets, but were not used due to their corrosive character. A series of refractive index matching fluids (manufactured by R.P.Cargille Labs. Inc., Cedargrove, NJ, USA) were used in the flow experiments. In order to adjust the refractive index of the operating liquid to match that of the glass fiber mat, a blend of two optical fluids was used. The liquids used were Cargille 5040 with refractive indices of 1.475 and 1.570 (at 25°C and 5893 A). A blending correlation was obtained for these through experiments. It is given by

$$\kappa_{mix} = \kappa_1 \varphi_1 + \kappa_2 \varphi_2$$

where κ_{mix} is the refractive index of mixture, and κ_i and φ_i are the refractive index and volume fraction of the i^{th} solution, respectively. Chloroparaffins (manufactured by Dover Chemical Corp.,Dover, OH 44622) with

refractive indices close to those of the optical solutions were blended with the optical solutions to vary the solution viscosities[7] .

Liquid viscosity was measured using a Couette geometry on a fluids spectrometer (Rheometrics Inc.) at four shear rates. The fluids were Newtonian; i.e., the viscosities were found to be independent of shear rate.

Wettability of the glass filaments was altered using fluorosurfactant surface treatments on the networks. Surface tension of the liquid and wettability of the filaments were determined using a modified Wilhelmy wetting force measurement technique that has been previously described[9].

Network Characteristics

The nonwoven multifilament glass network is characterized in terms of the following parameters:

Average or bulk porosity (ε):

$$\varepsilon = 1 - \frac{m}{\rho_g h}$$

where m is mass per unit mat area, ρ_g is the density of the glass filaments, and h is the spacing between the plates of the radial flow cell (mat thickness). Average porosity of the mats fluctuated within about 4-5% (Appendix 1).

Average permeability:

This was determined using the TRI radial in-plane permeability measurement technique[10]. The mats used were found to be isotropic with an average permeability of about 1000 darcy.

Pore Volume Distribution:

Pore structure of the mats was characterized by the liquid extrusion method on the TRI Pore Volume Distribution apparatus[11] .

EXPERIMENTAL WORK

Radial in-plane flow experiments were carried out at constant inlet flow rates using three types of mats. These differed in their average filament diameter, and the type of surface sizing. Refractive indices of the filaments ranged between 1.550 and 1.552 for the three mats. Care was taken in choosing samples to minimize variability in their average porosity. Mats of type I were compressed to a thickness of 0.05×10^{-2} m corresponding to a porosity of 0.76, and similarly those of type II and type III, to a thickness of 0.08×10^{-2} m corresponding to a porosity of 0.82 and 0.83 respectively. The experiments spanned a range of inlet volumetric flow rates from 0.15×10^{-6} to 0.75×10^{-6} m^3/s providing a range of interstitial velocities. Liquid viscosities ranged from 45×10^{-3} to 290×10^{-3} Pa.s and surface tensions varied from 28×10^{-3} to 36×10^{-3} N/m.

Studies were carried out on mats of type III, after treating these with a series of surfactants. This changed the wettabilities of filaments composing the mats without varying the fluid properties or the network structure. The surface treatments were carried out by saturating a mat with a surfactant solution in a bath for 10 minutes, followed by air drying. The wettability of these treated surfaces was measured in terms of an equilibrium contact angle formed by the test fluid on the surface. Contact angle values ranged from 20^o (wetting) to 78^o (nonwetting). Table 1 summarizes the different surfactant solutions and the corresponding equilibrium contact angles formed by the test fluids with the filament surface after treatment. Measured contact angle values were averages taken over a random set of 5-6 filaments that were picked out of the surface treated mats.

An attempt was made to study the effect of spatial variations in permeability on air entrapments by imposing known deformities onto the already existing mat structure. Deformation and reorientation was imposed by impinging the mat on a regular rectangular grid of 3 mm. diameter pegs. The reoriented filaments were held in place by exposing the mat to vapors of super glue in the presence of moisture. A schematic of this apparatus is shown in Figure 2. The resultant mat had a uniform spatial distribution of large pores at the location of pegs imposed on the isotropic random structure.

RESULTS AND DISCUSSION

Effect of Capillary Number

Forced flow through fiber networks results from a combination of viscous and surface tension effects. A dimensionless number quantifying the relative magnitude of viscous forces to interfacial forces is the capillary number (Ca) which is defined as follows:

$$Ca = \frac{\mu v}{\gamma}$$

where μ is viscosity, γ is surface tension, and v is interstitial velocity of fluid.

Velocity and viscosity effects on the extent of entrapment, when combined through the capillary number, collapse on to single master curves for mats I, II and III. These are shown as plots of void fraction as a function of capillary number in Figures 3,4 and 5. For all three mat types there is a critical value of capillary number which identifies a zone below which void content increases exponentially with decreasing capillary number. Above this value, negligible entrapment is observed. The critical capillary number at the onset of void formation is 2.5×10^{-3}. Although the volume fraction of trapped voids is roughly comparable for mats I, II and III, the voids in mat II are larger than those in mats I and III. There is also more variability in the results for mat II than for mats I and III.

Sizes of the entrapped regions spanned a wide range, from tiny spherical bubbles (completely trapped in single pores) to larger irregular shaped zones (encompassing several pores).The number fraction of small entrapments [x_1] increases with increasing fluid velocity. At the same time the number fraction of intermediate sized regions [x_2] and the number fraction of larger sized regions [x_3] decreases with increasing fluid velocity, as shown in Figures 6,7 and 8. Viscosity of the liquid also has a strong influence on x_i as shown in Figure 9.

The data from Figure 9 collapse onto a single curve when the velocity and viscosity effects are combined in terms of the capillary number, as shown in Figure 10. Comparable curves for x_2 and x_3 are shown in Figures 11 and 12. Lower capillary numbers favor formation of larger sized entrapments as opposed to the smaller sized ones. The smaller sized entrapments are of the order of the mean pore size in the mat. These entrapments are usually located completely inside a pore and are spherical in shape. Larger sized entrapments span more than a single pore.

Effect of Filament Wettability

It is known from previous work in fluid displacement mechanics in porous media that there is a significant difference between wetting displacement ($\cos\theta = 1$) and non-wetting displacement ($\cos\theta = 0$)[12]. Studies have indicated that poor resin wettability of commercial finished filaments resulted in an increase in the formation of voids[6]. Reducing the contact angle to zero and/or oscillating the tension in the strand as it passed through the resin markedly reduced the number of voids.

Flow experiments carried out using surface treated mats covered a range of contact angles between 20^{o} and 78^{o}. Figure 13 shows void fraction as a function of capillary number for different surface treatments. As seen from these plots, no particular trend in the slope of the curve or in the critical capillary number value is

observed with respect to the surface wettability up to an angle of 57^{o}. Beyond this, as the angle approaches 90^{o}, air entrapment drops to zero; within the same range of capillary numbers. This suggests a critical transition between a zone of entrapment to that of no entrapment as the surface wettability of the filaments composing the mat structure decreases. This result along with the observations of Bascom and Romans[6] suggests that entrapment is high under conditions of extremely low as well as extremely high wettabilities; and is minimal at intermediate contact angles that are close to 90^{o}. Local nonuniformities are one cause of entrapment. The local shape of meniscus between filaments is flatter and has less curvature at contact angles close to 90^{o}, whereas it is sharply curved for angles close to 0^{o} and 180^{o}.

A study carried out on the effect of filament wettabilities on the size distribution of entrapped zones indicates that size distribution data for the range of capillary numbers obtained for different surface wettabilities collapses onto a single curve when plotted against a modified capillary number.

The modified capillary number is expressed as given below:

$$Ca = \frac{\mu v}{\gamma \cos\theta}$$

where θ is the equilibrium contact angle made by the liquid with the filaments composing the network. Experimental data indicating the effect of modified capillary number on void sizes are given in Figures 14, 15 and 16.

Effect of Mat Structure:

The nonwovens used here have groups of filaments bundled together. These bundles are placed randomly to create a structure having a bimodal pore volume distribution, as shown in Figure 17. The smaller pores are created by the spacing between filaments. The larger ones are the pores between multifilament bundles.

In the process of deforming and reorienting the pore structure with the grid of pegs, the filaments are relocated to create open spaces or holes. Hence the structure is modified to have three types of pores. The original bimodal structure still exists along with a third type of pores created by the pegs. The pore volume distribution plot for this deformed network is also shown in Figure 17. The third peak representing the newly created pores is not observed in this measurement. Calculation using the dimensions of the grid indicates that the total volume of large pores created in this restructuring process is 8% of the total pore volume (Appendix 2). The deformation therefore, is insufficient to appear as an additional peak in the pore volume distribution diagram. The results of flow experiments on these deformed mats is the same as those on undeformed mats. These are shown in Figure 18; and simply reproduce results from experiments carried out on undeformed samples that are shown in Figure 5.

CONCLUSIONS

The isorefractive index technique combined with an image analysis system was found to be an elegant method of quantifying air entrapment in glass filament networks. When applied to radial flow geometry, this technique was useful in mapping voids and hence relating them to interstitial velocity and viscosity of the penetrating liquid. The technique provides data that will be useful in designing impregnation and mold filling processes for the production of advanced composite materials. A critical capillary number for void formation was found to be 2.5×10^{-3}. Below the critical capillary number the volume fraction of trapped voids increases exponentially with capillary number. Surface wettability of filaments composing a nonwoven mat measured in terms of an equilibrium contact angle, affects the fluid flow mechanism. Experiments indicate that there is a critical contact angle between 57^{o} and 78^{o} above which air entrapment is minimal. Below this value, there is no change in the relationship between void fraction and capillary number. A modified capillary number that includes the equilibrium contact angle seems to control the mean size of entrapments. Definite answers are yet to be arrived at which would quantitatively express the effect of network properties on void formation.

ACKNOWLEDGMENT

The assistance of Mrs. Susan M. Montgomery of TRI/Princeton with the image analysis system is gratefully acknowledged.

APPENDIX 1

Estimation of bulk porosity variation:

Variation in bulk porosity is related to the variation in specific mass by:

$$[\varepsilon + \Delta\varepsilon] = 1 - [\frac{m + \Delta m}{\rho_g h}]$$

Maximum variation of mass in samples used with one operative liquid was 10 Kg/0.0225 m^2 [Δm] for an average mass of 70 Kg/0.0225 m^2 [m], ρ_g is of magnitude 2560.0 Kg/m^3, and the smallest value of spacing [h] used was 0.05×10^{-2}m.

Using these values, variation in bulk porosity is given by:

$$\frac{[\varepsilon + \Delta\varepsilon] - [\varepsilon]}{[\varepsilon]} \times 100 = [\frac{-\Delta m}{\rho_g h - m}] \times 100$$

$$= 4.6\%$$

APPENDIX 2

Estimation of porosity created by deformation:

$$\varepsilon = 1 - \frac{V_g}{V_t}$$

$$\varepsilon h = \frac{V_h}{V_t}$$

$$V_g = \frac{m_t}{\rho_g}$$

Substituting in above the values of:

$$m_t = 7.4 \times 10^{-3} \text{ Kg}$$

$$\rho_g = 2.56 \times 10^3 \text{ Kg/m}^3$$

$$V_t = 225x0.08x10^{-6}\ m^3$$

$$V_g = 225x0.08x\Pi x(0.15)^2x10^{-6}\ m^3$$

$$\varepsilon t = 0.84$$

$$\varepsilon h = 0.06$$

Therefore the percentage of total porosity due to the deformation is given by:

$$\frac{\varepsilon h}{\varepsilon t}x100 = 7.1\%$$

REFERENCES

1. E.J.Kohn, A.G.Sands and R.C.Clark, Ind. and Eng. Chem. Product Research and Development, 7, 179 (1968).

2. N.C.Judd and W.W.Wright, SAMPE, **14**, No1, 10 (1978).

3. W.Hand, Proceedings of the 20th Technical Conference, SPI Reinforced Plastics Division, Section 1-E,Feb(1965).

4. J.T.Paul and J.B.Thomson, Proceedings of the 20th Technical Conference, SPI Reinforced Plastics Division, Section 12-C,Feb(1965).

5. I.Petker, Soc. Plastic Eng. Trans,49 (1965).

6. W.D.Bascom and J.B.Romans, Ind. and Eng. Chem. Product Research and Development, **7**, 172 (1968).

7.A.D.Mahale, R.K.Prud'homme, L.Rebenfeld, Polymer Eng. & Sci.,**32** ,No 5, 319 (1992).

8. J.McAdams, Rev. Sci. Instrum. **59** (12), 2617 (1988).

9. B.Miller, in *Absorbency*, edited by P.K.Chatterjee (Elsevier, New York) (1985).

10. K.L.Adams, B.Miller, L.Rebenfeld, Polymer Eng. & Sci.,**26**, 1434 (1986).

11. B.Miller, I.Tyomkin, Textile Research Jnl., **56**, No 1,35 (1986).

12. D.Wilkinson, American Physical Society, Physical Review A., **34**, No 2, 1380 (1986).

TABLE 1

SURFACE TREATED SAMPLES

Viscosity = 48 cp. Surface tension = 34 dynes/cm.

cos θ	θ	Surface treatments used
0.2	78	100 ppm Zonyl FSC solution.
0.55	57	0.05% w/w Sodium Laurel Sulfate.
0.64	50	0.1% w/w Sodium Laurel Sulfate.
0.67	48	100 ppm Zonyl FSN solution.
0.90	25	no treatment.

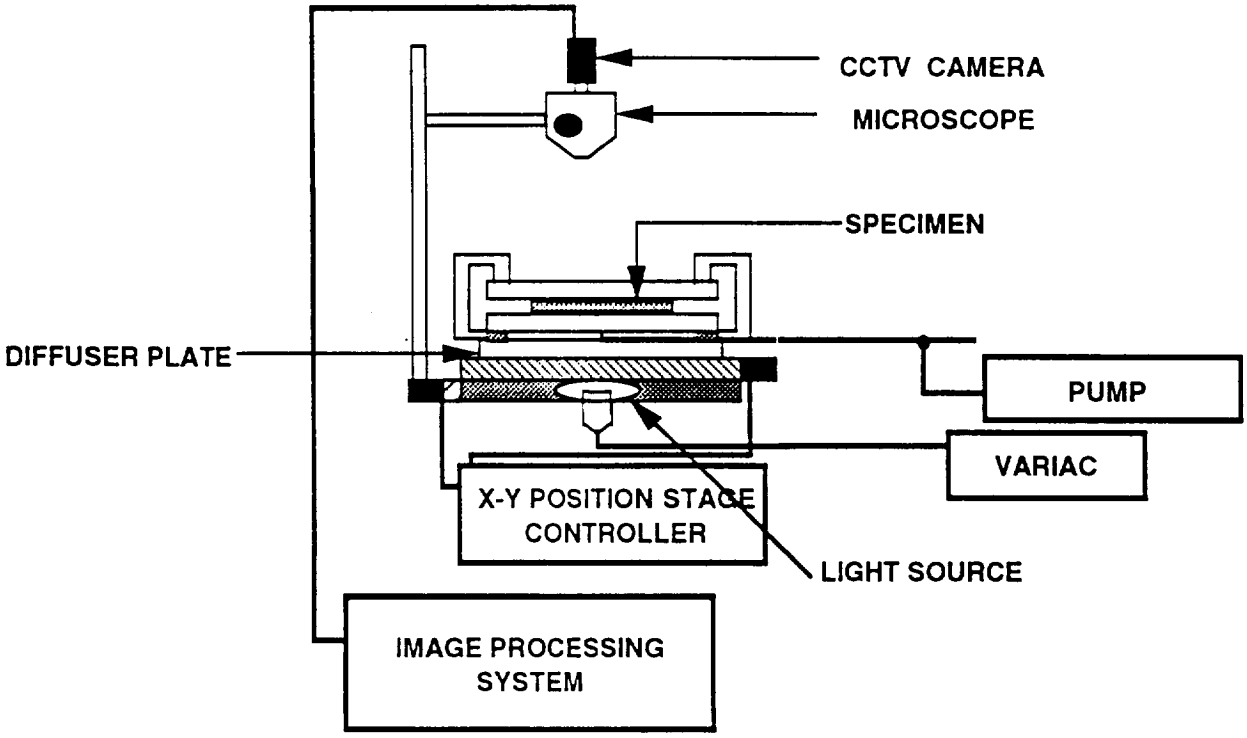

EXPERIMENTAL APPARATUS

FIG 1

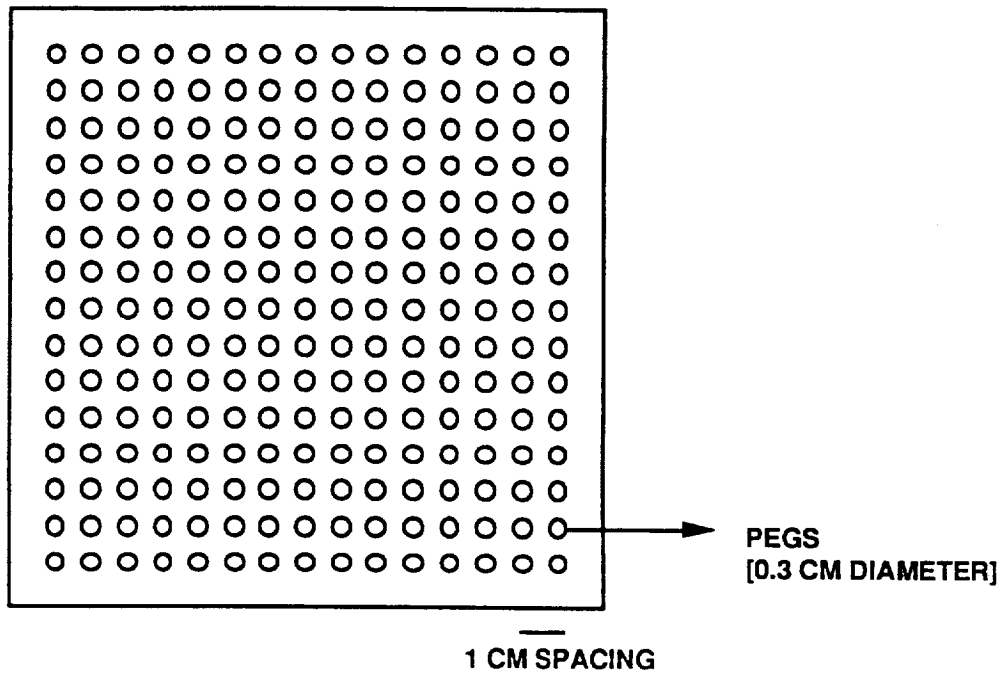

GRID OF PEGS

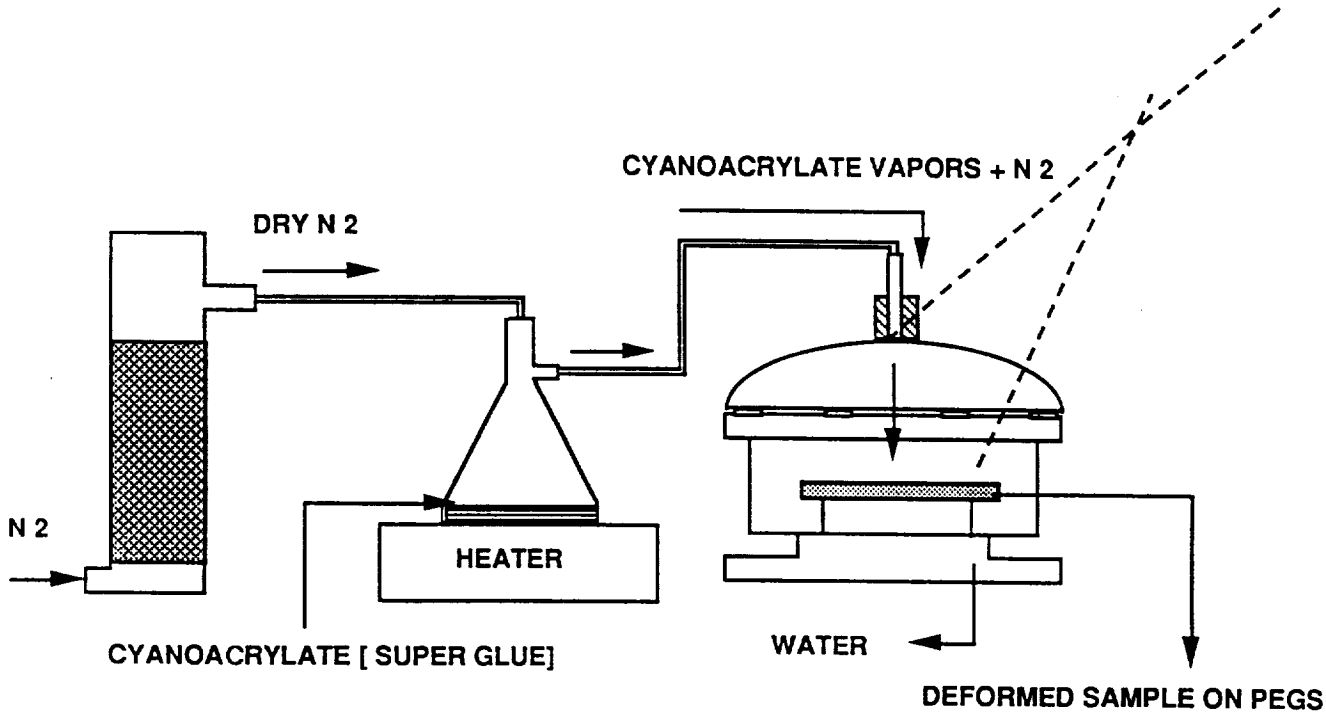

THE PROCEDURE FOR REORIENTATION OF MAT STRUCTURE.

FIG 2

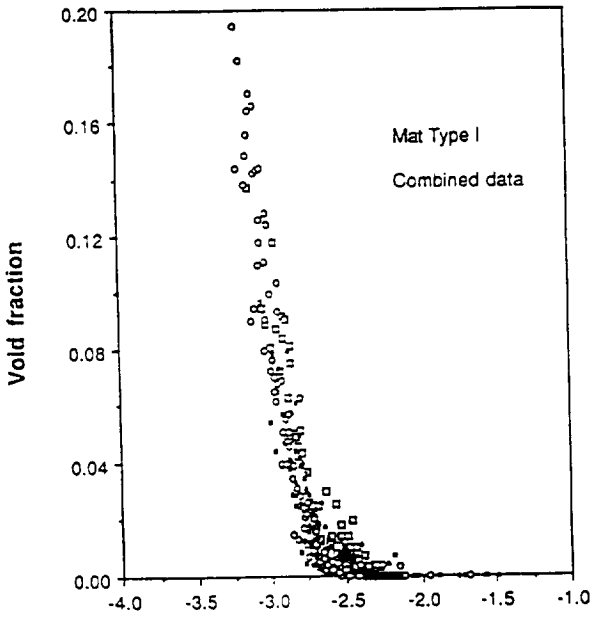

Void fraction vs Capillary number

FIG 3

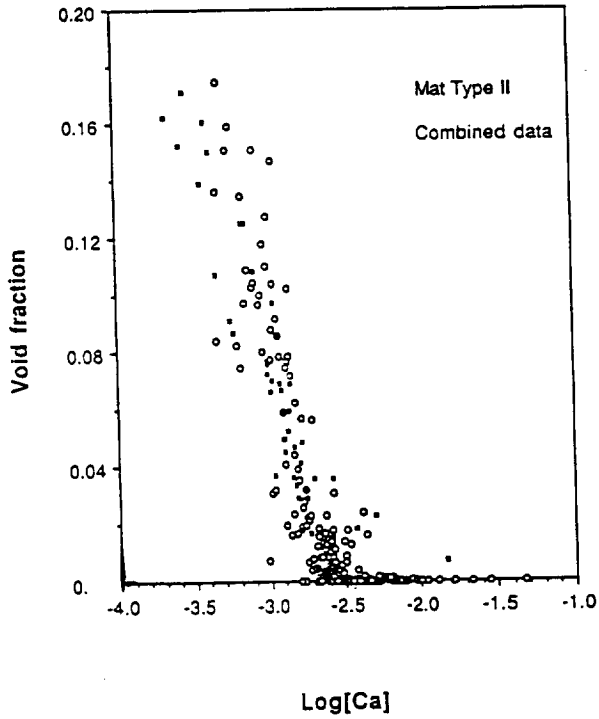

Void fraction vs Capillary number

FIG 4

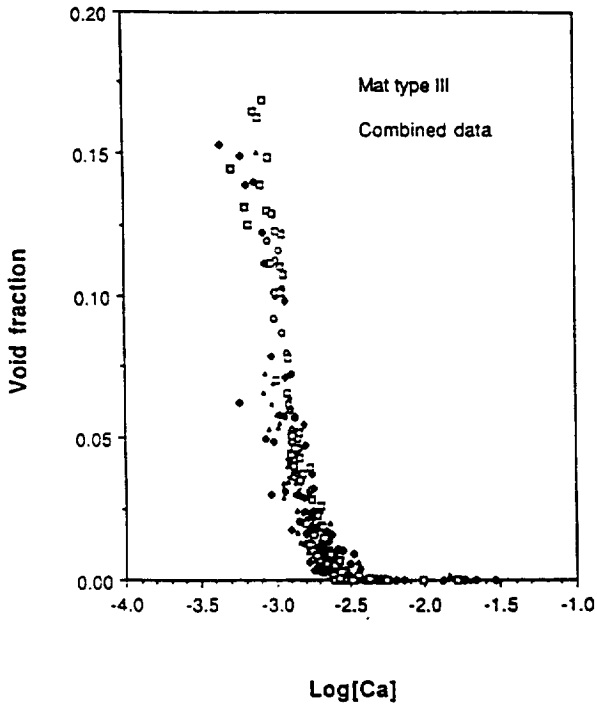

Void fraction vs Capillary number

FIG 5

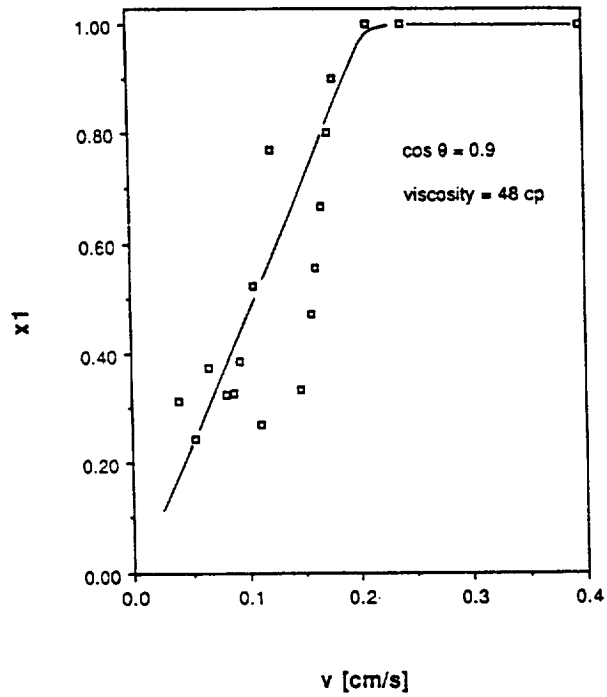

Fraction of total number of bubbles in the range of sizes < 0.32 mm3

FIG 6

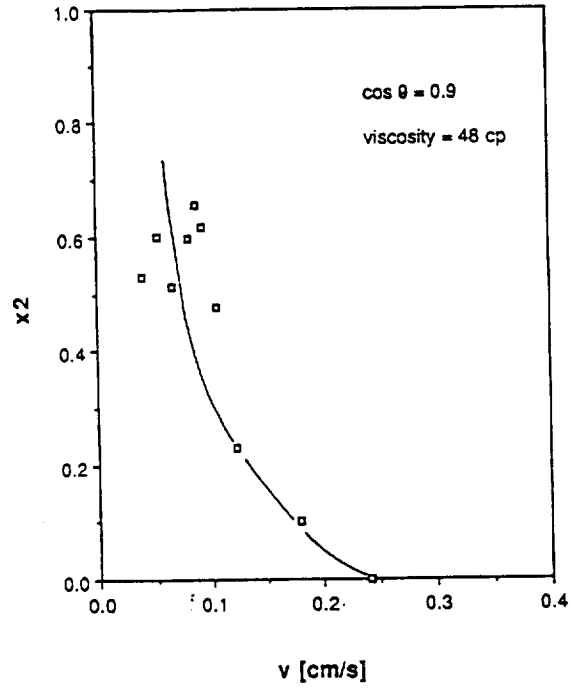

Fraction of total number of bubbles in the range of 0.32 - 1.9 mm3

FIG 7

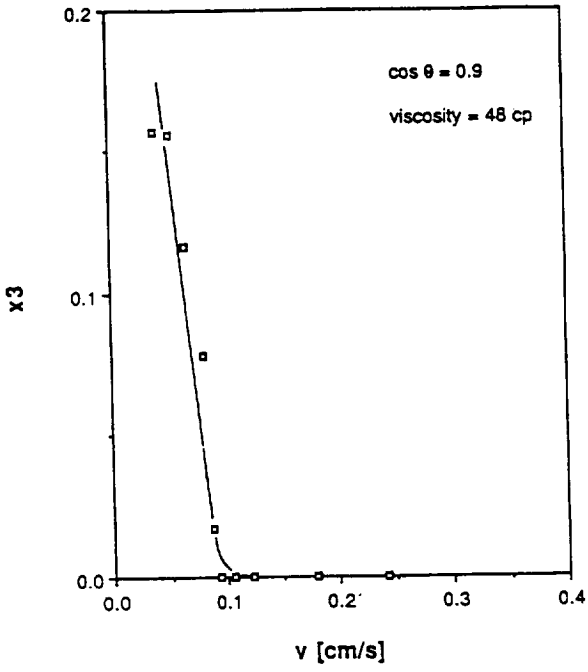

Fraction of total number of bubbles in the range of sizes > 1.9 mm3

FIG 8

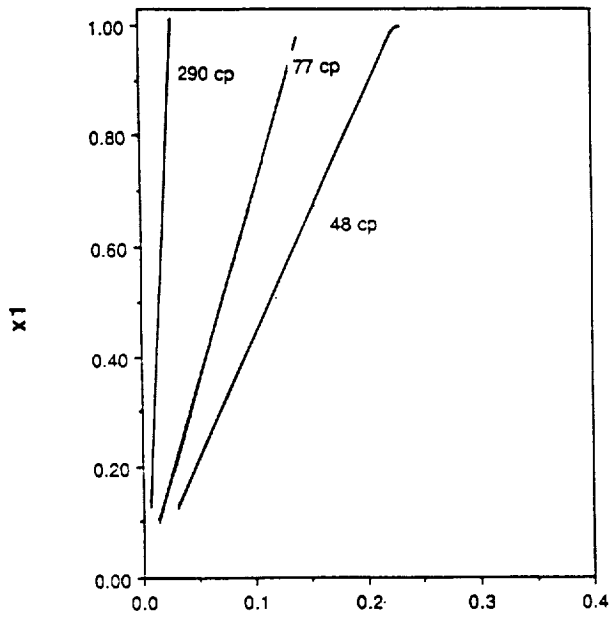

Fraction of total number of bubbles in the range of sizes < 0.32 mm3

FIG 9

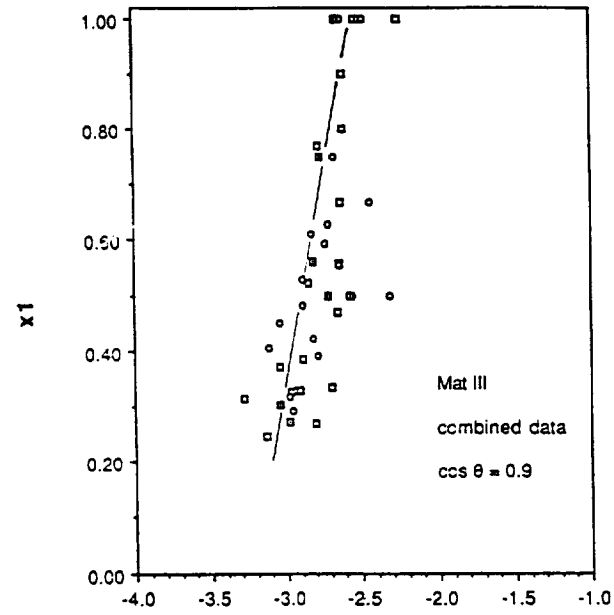

X1 vs Capillary number

FIG 10

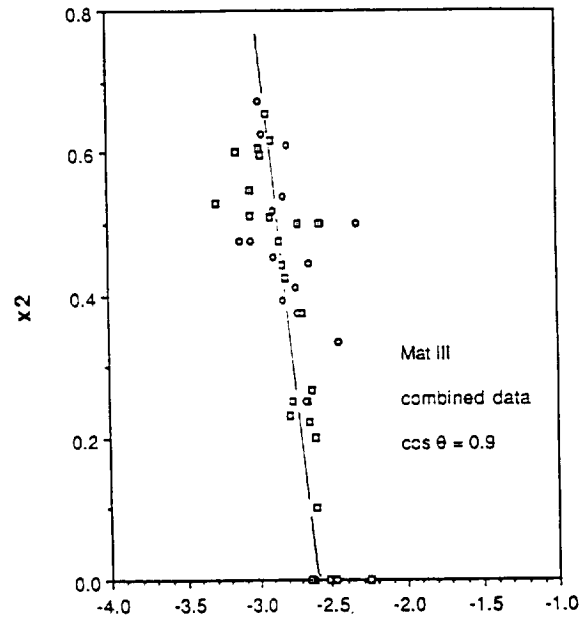

X2 vs Capillary number

FIG 11

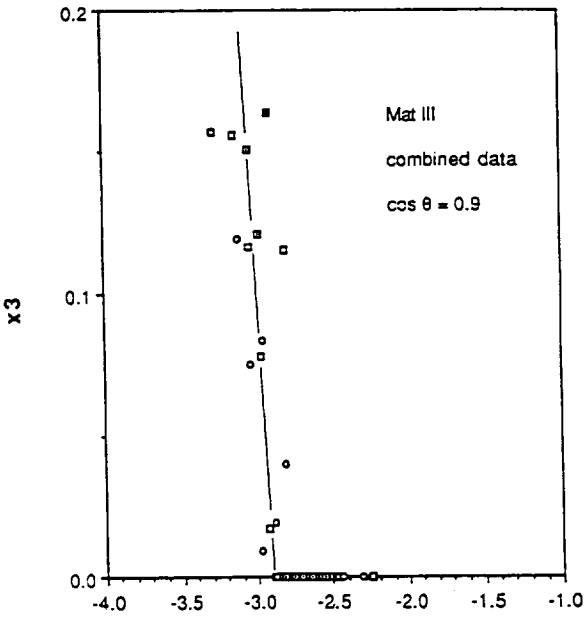

X3 vs Capillary number

FIG 12

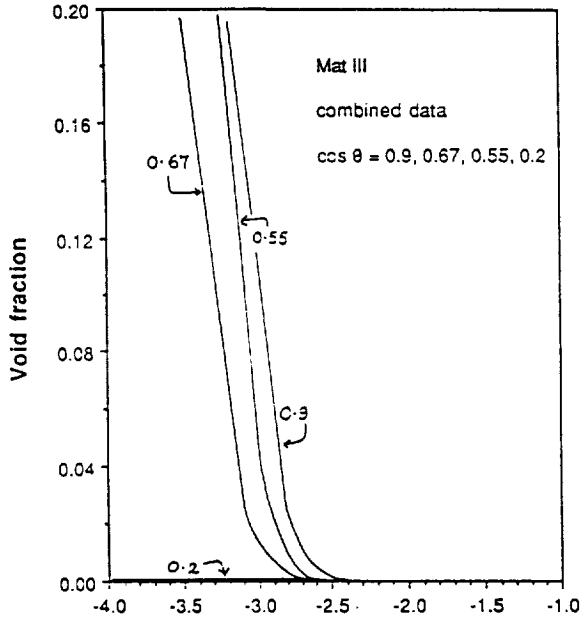

Void fraction vs Capillary number

FIG 13

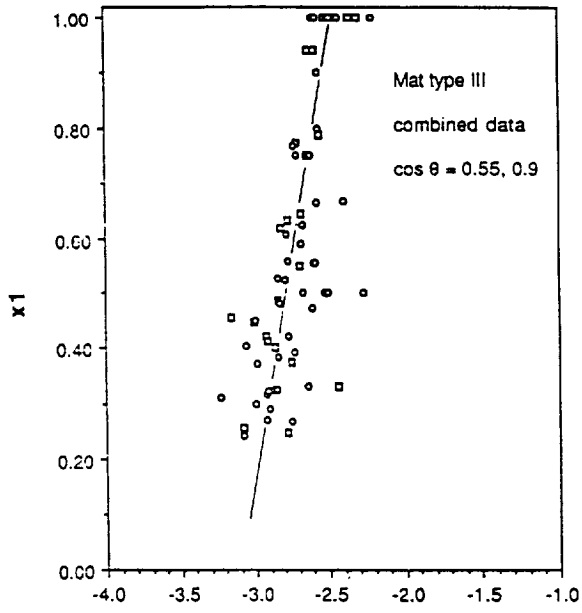

X1 vs Modified Capillary number

FIG 14

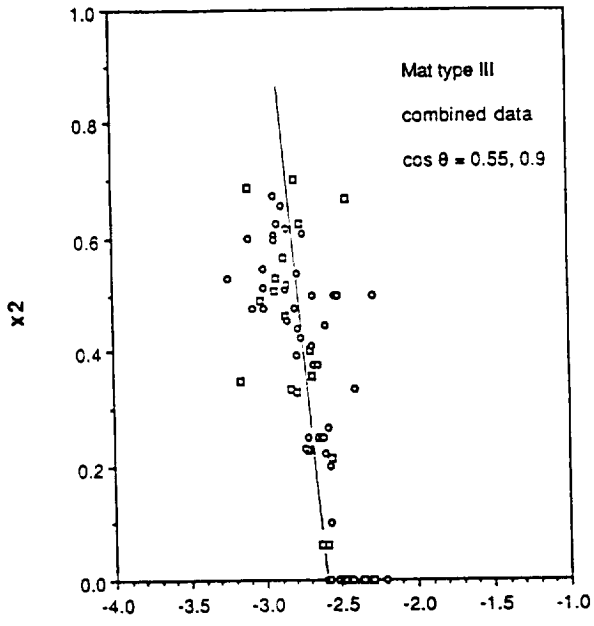

X2 vs Modified Capillary number

FIG 15

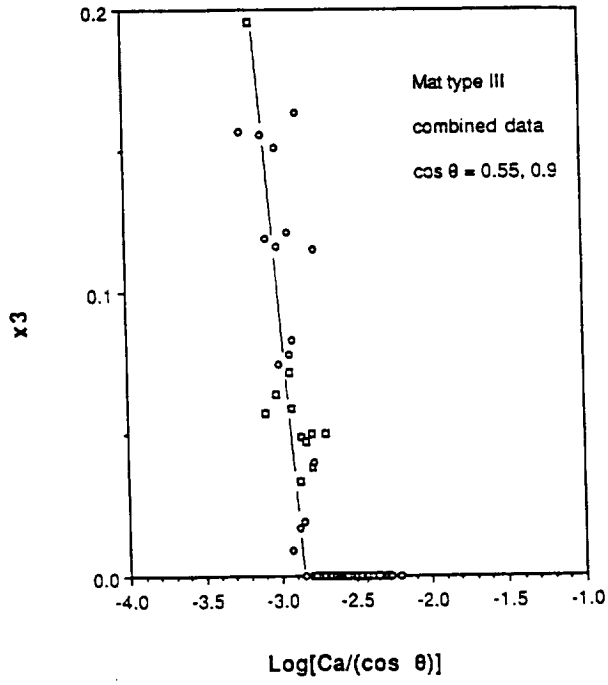

X3 vs Modified Capillary number

FIG 16

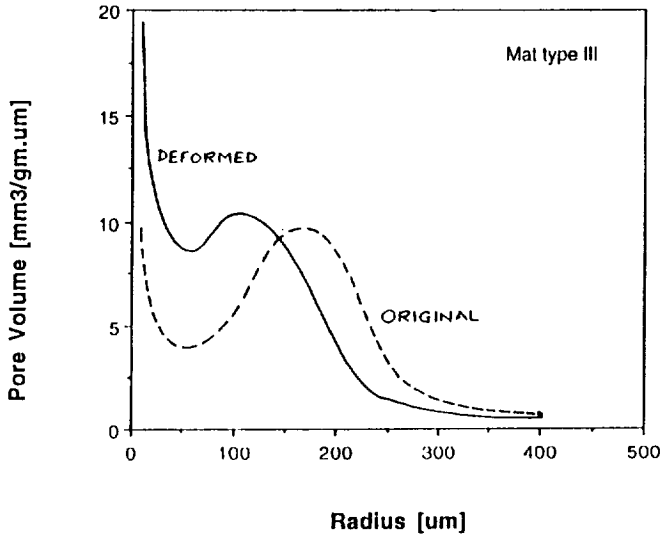

Pore Volume Distribution

FIG 17

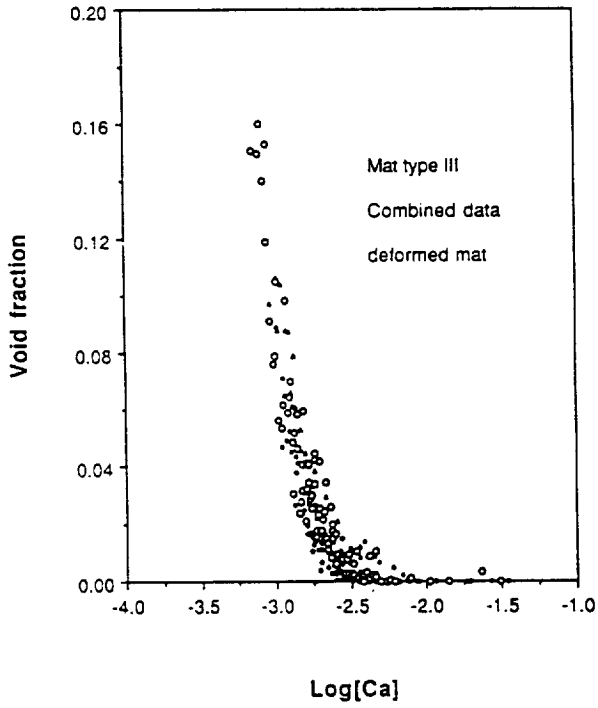

Void fraction vs Capillary number

FIG 18